Adaptive Guaranteed Performance Control of Wind Energy Systems

Wenchao Meng and Qinmin Yang

Abstract In this chapter, we present an adaptive guaranteed performance controller for wind energy conversion system (WECS) equipped with doubly fed induction generator (DFIG). The proposed controller consists of outer loop control concerning the aeroturbine mechanical subsystem, and inner loop control concerning the electrical subsystem. As opposed to most existing studies, we are capable of quantifying and further guaranteeing the system performance on both transient and steady state stages with the help of error transformation techniques. The stability is guaranteed via standard Lyapunov synthesis. Finally, the effectiveness of the proposed scheme is validated on a 1.5 MW DFIG-based wind turbine using the FAST (Fatigue, Aerodynamics, Structures, and Turbulence) simulator developed by the National Renewable Energy Laboratory (NREL).

Nomenclature

ρ	Air density
V	Wind speed
R	Rotor radius
C_p	Power coefficient
$C_q(\lambda, \beta)$	Torque coefficient
β	Pitch angle
λ	Tip-speed ratio
P_r	Rotor power
T_a	Aerodynamic torque
J_r, J_g	Rotor and generator inertias
K_r, K_g	Rotor and generator external damping
T_{hs}, T_{ls}	High-speed and low-speed torque

W. Meng · Q. Yang (✉)
College of Control Science and Engineering, Zhejiang University,
Hangzhou Zhejiang 310027, People's Republic of China
e-mail: qmyang@zju.edu.cn

W. Meng
e-mail: wmengzju@gmail.com

R.-E. Precup et al. (eds.), *Advanced Control and Optimization Paradigms for Wind Energy Systems*, Power Systems, https://doi.org/10.1007/978-981-13-5995-8_6

T_{em}	Electromagnetic torque
n_{ra}	Gearbox ratio
Ω_r	Rotor speed
$\Phi_{d,qs}$	Stator flux
$\Phi_{d,qr}$	Rotor flux
$U_{d,qs}$	Stator winding voltage
$U_{d,qr}$	Rotor winding voltage
$I_{d,qs}$, $I_{d,rq}$	Stator and rotor winding currents
L_s, L_r	Self-inductance of the stator and rotor
L_m	Mutual inductance between windings
R_s, R_r	Resistance of the stator and rotor
Ω_s	Frequency of the grid
p	Number of pole pairs
$V_{cut\text{-}in}$	Cut-in wind speed
$V_{cut\text{-}off}$	Cut-off wind speed
V_{rated}	Rated wind speed

1 Introduction

In recent years, the wind energy conversion systems have received more and more attentions from both academic and industrial communities due to the depletion of tradition energy source and increasing environment pollution [1, 2]. Because of this, the WECS has experienced the fastest growth and this tendency is expected to endure for a long time [3, 4]. However, it is still provide a very small share in the global energy market due to its high costs, and developing advanced control algorithms is considered to be a promising way to reduce its costs.

Linear control methods have been commonly used for control of wind energy conversion systems [5, 6]. The linear methods only deliver satisfactory performance when the plant works around the corresponding operation point, whereas the operation point of WECS changes frequently because of the random wind. Therefore, the system performance will be impaired if the linear method is enforced.

In order to avoid the drawbacks of linear methods, many nonlinear control methods have been studied [7, 8]. However, in previous studies, only steady state performance of the control system has been taken into account, while the more essential transient performance has been rarely considered.

Therefore, in this chapter, an adaptive guaranteed performance control is proposed for WECS equipped with DFIG. The proposed controller includes two loops [9, 10], i.e., the outer loop control and inner loop control. The outer loop control concerns the aeroturbine mechanical subsystem while the inner loop control concerns the electrical subsystem. Compared with most existing studies, performance indexes including steady-state error, convergence rate and overshoot are guaranteed.

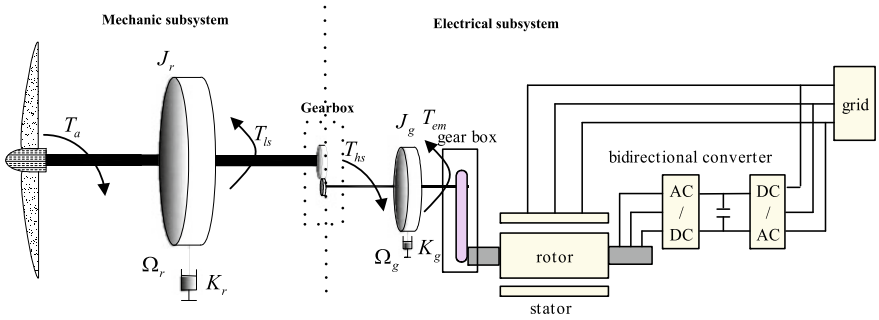

Fig. 1 Wind energy conversion system

2 Wind Energy Conversion System

The wind energy conversion system includes the mechanical subsystem and electrical subsystem as depicted in Fig. 1. For the mechanical subsystem, the rotor power extracted from wind can be formulated as [11]

$$P_r = \frac{1}{2}\rho\pi R^2 C_p(\lambda, \beta)V^3 \tag{1}$$

The tip-speed ratio λ is defined by

$$\lambda = \frac{R\Omega_r}{V} \tag{2}$$

The rotor power P_r can also be formulated as

$$P_r = \Omega_r T_a. \tag{3}$$

with

$$C_q(\lambda) = \frac{C_p(\lambda)}{\lambda} \tag{4}$$

Invoking (3), (4) and (1), we have

$$T_a = \frac{1}{2}\rho\pi R^3 C_q(\lambda)V^2 \tag{5}$$

The rotor dynamics together with the generator dynamics can be written as

$$J_r\dot{\Omega}_r = T_a - K_r\Omega_r - T_{ls} \tag{6}$$

$$J_g\dot{\Omega}_g = T_{hs} - K_g\Omega_g - T_{em} \tag{7}$$

The gearbox ratio n_{ra} is defined as

$$n_{ra} = \frac{\Omega_g}{\Omega_r} = \frac{T_{ls}}{T_{hs}} \tag{8}$$

Substituting (8) into the generator dynamic (7), we have

$$n_{ra}^2 J_g \dot{\Omega}_r = T_{ls} - \left(n_{ra}^2 K_g\right) \Omega_r - n_g T_{em} \tag{9}$$

Thereafter, a simple model of the mechanic subsystem can be obtained as

$$J_o \dot{\Omega}_r = T_a - K_o \Omega_r - T_g \tag{10}$$

where

$$\begin{cases} J_o = J_r + n_{ra}^2 J_g \\ K_o = K_r + n_{ra}^2 K_g \\ T_g = n_{ra} T_{em} \end{cases} \tag{11}$$

The generator power can be formulated as

$$P_g = T_g \Omega_r \tag{12}$$

For the electrical subsystem, we consider the doubly-fed induction generator which connects directly to the grid through the stator, while the rotor winding is interfaced through a bidirectional power electronic converter. In this kind of wound-rotor machine, the power system electrical frequency and the rotor mechanical frequency can be decoupled, which makes a variable speed operation of the wind turbine possible. One of the main advantages is that it can generate and deliver electrical power at the frequency and voltage demanded by the grid. Inspired by [12], the model of DFIG in the Park $d-q$ frame is given by

$$\begin{cases} \dot{\Phi}_{d,s} = U_{d,s} - R_s I_{d,s} + \Omega_s \Phi_{q,s} \\ \dot{\Phi}_{q,s} = U_{q,s} - R_s I_{q,s} - \Omega_s \Phi_{d,s} \\ \dot{\Phi}_{d,r} = U_{d,r} - R_r I_{d,r} + \left(\Omega_s - p\Omega_g\right) \Phi_{q,r} \\ \dot{\Phi}_{q,r} = U_{q,r} - R_r I_{q,r} - \left(\Omega_s - p\Omega_g\right) \Phi_{d,r} \end{cases} \tag{13}$$

with

$$\begin{aligned} \Phi_{d,s} &= L_s I_{d,s} + L_m I_{d,r} \\ \Phi_{q,s} &= L_s I_{q,s} + L_m I_{q,r} \\ \Phi_{d,r} &= L_r I_{d,r} + L_m I_{d,s} \\ \Phi_{q,r} &= L_r I_{q,r} + L_m I_{q,s} \end{aligned} \tag{14}$$

Inspired by [12], a simplified generator model can be given by

$$\dot{I}_{d,r} = \left(\Omega_s - p\Omega_g\right) I_{q,r} - \frac{L_s R_r}{L_e} I_{d,r} + \frac{L_s}{L_e} U_{d,r} + \varpi_d(t) \tag{15}$$

$$\dot{I}_{q,r} = -\frac{L_s R_r}{L_e} I_{q,r} - \left(\Omega_s - p\Omega_g\right)\left(I_{d,r} + \frac{L_m V_s}{L_e \Omega_s}\right) + \frac{L_s}{L_e} U_{q,r} + \varpi_q(t) \tag{16}$$

where V_s is the grid voltage and $L_e = L_s L_r - L_m^2$. The terms $\varpi_d(t), \varpi_q(t)$ are added to represent bounded disturbances [13]. Thereafter, the currents of stator can be algebraically calculated as

$$\begin{aligned} I_{d,s} &= \frac{V_s}{\Omega_s L_s} - \frac{L_m}{L_s} I_{d,r} \\ I_{q,s} &= -\frac{L_m}{L_s} I_{q,r} \end{aligned} \tag{17}$$

The electromagnetic torque along with reactive power is given by

$$T_{em} = -\frac{3}{2} p \frac{V_s L_m}{\Omega_s L_s} I_{q,r} \tag{18}$$

$$Q = \frac{3V_s^2}{2\Omega_s L_s} - \frac{3V_s L_m I_{d,r}}{2L_s} \tag{19}$$

3 Problem Formulation

There are two operation regions for the wind turbine, namely, below the low-speed region and high-speed region as given in Fig. 2 [14, 15].

- Low-speed region: where $V_{cut\text{-}in} \leq V < V_{rated}$ and $P_g < P_{rated}$.
- High speed region: where $V_{rated} \leq V \leq V_{cut\text{-}off}$ and $P_g = P_{rated}$.

In low-speed region, the desired power is given by

$$P_g^* = n_p P_r^{\max} \tag{20}$$

with

$$P_r^{\max} = \frac{1}{2} \rho \pi R^2 C_p^{\max} V^3 \tag{21}$$

Notice that the response of the WT electrical subsystem is much faster than that of the mechanical part of the WT. Hence, the controller design for the electrical subsystem and mechanical subsystem is usually decoupled and a cascaded control structure containing two control loops is usually adopted as shown below

- The outer control loop concerns the aeroturbine mechanical subsystem.
- The inner control loop concerns the electrical subsystem.

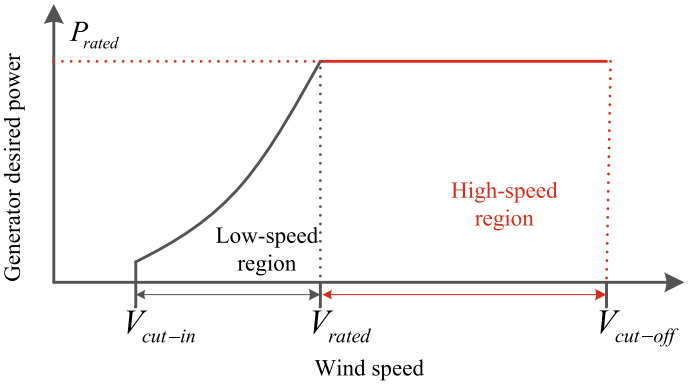

Fig. 2 Generator desired power curve

Because the aeroturbine runs much slower than electrical subsystem, the state of the outer loop can be seen as a slow changing disturbance while calculating the control signal for the inner loop. In the meantime, the outer loop controller is usually designed based on the assumption that the inner electrical control loop is able to track the reference T^* timely. It implies that the stability analysis in the outer control loop and inner control loop can be addressed separately in literature [16].

In this chapter, we consider the low-speed operation region. For the outer control loop, our main goal is to design appropriate generator torque T_g such that P_g can track P_g^*. For the inner control loop, the control objective is to design input voltages $U_{d,r}, U_{q,r}$ such that: (1) the electromagnetic torque T_{em} tracks its reference T^*, and (2) the reactive power Q follows its desired value Q^*.

For analysis convenience, we define the following tracking errors

$$\ell_o = P_g^* - P_g \tag{22}$$

$$\ell_{i,T} = T_{em} - T^* \tag{23}$$

$$\ell_{i,Q} = Q - Q^* \tag{24}$$

4 Outer Loop Control

In the outer control loop, both the transient and steady state performance will be considered. Specifically, the imposed performance requirements on $\ell_o(t)$ are

P1:

- The steady tracking error $\ell_o(\infty)$ is required to be within $-\eta_o \hbar_o(\infty) \leq \ell_o(\infty) \leq \hbar_o(\infty)$.
- It converges faster than the signal $\hbar_o(t)$.
- The maximum overshoot is required to be smaller than $\eta_o \hbar_o(0)$.

For evaluating the prescribed performance, the following performance function is firstly introduced.

Definition 1 ([17]) A performance function is a smooth function $\hbar_o(t) : \Re^+ + \{0\} \to \Re^+$ that satisfies $|\ell_o(0)| < \hbar_o(0)$ and $\lim_{t\to\infty} \hbar_o(t) = \hbar_o(\infty) > 0$.

Assume $0 \leq \ell_o(0) < \hbar_o(0)$, if the tracking error satisfies

$$-\eta_o \hbar_o(t) < \ell_o(t) < \hbar_o(t) \tag{25}$$

with $0 \leq \eta_o \leq 1$ being a design parameter, the prescribed performance P1 can be attained.

To proceed the prescribed performance design, an error transformation in [17], which can convert the original error with imposed performance requirements into a new error without imposed performance requirements, will be introduced. Specifically,

$$\ell_o(t) = \hbar_o(t) M_o(\gamma_o) \tag{26}$$

or

$$\gamma_o(t) = {M_o}^{-1}\left(\frac{\ell_o(t)}{\hbar_o(t)}\right) \tag{27}$$

with γ_o being the new error, and $M_o(\cdot)$ is a function that is smooth and strictly increasing. The function $M_o(\cdot)$ is required to satisfy

$$\begin{cases} \lim_{\gamma_o\to-\infty} M_o(\gamma_o) = -\eta_o \\ \lim_{\gamma_o\to\infty} M_o(\gamma_o) = 1 \end{cases} \tag{28}$$

where ${M_o}^{-1}(\cdot)$ is the inverse function of $M_o(\cdot)$. There exist many choices for the function $M_o(\gamma_o)$, and a typical choice can be given as

$$M_o(\gamma_o) = \frac{{d_o}^{\gamma_o} - \eta_o {d_o}^{-\gamma_o}}{{d_o}^{\gamma_o} + {d_o}^{-\gamma_o}} \tag{29}$$

with $d_o > 1$. The function $M_o(\gamma_o)$ is demonstrated in Fig. 3.

The following fact holds as long as $\gamma_o(t)$ exists

$$-\eta_o < M_o(\gamma_o) < 1 \tag{30}$$

The above fact implies (25). It means that the imposed performance requirements in P1 are achieved. Thence, the control task becomes finding a control law to ensure the boundedness of γ_o. For this, by recalling (12), the time derivative of ℓ_o is

$$\dot{\ell}_o = \dot{P}_g^* - \dot{P}_g = \dot{P}_g^* - T_g \dot{\Omega}_r - \dot{T}_g \Omega_r \tag{31}$$

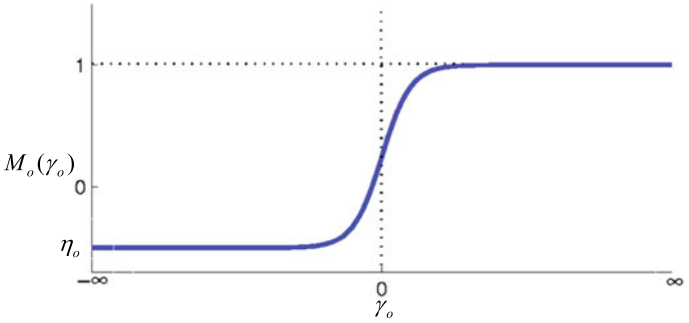

Fig. 3 Graphical illustration of the $M_o(\gamma_o)$ function

Thereafter, by differentiating (27) with respect to time, we have

$$\begin{aligned}\dot{\gamma}_o &= \frac{\partial {M_o}^{-1}}{\partial\left(\frac{\ell_o(t)}{\hbar_o(t)}\right)}\frac{1}{\hbar_o(t)}\left(\dot{\ell}_o(t) - \frac{\ell_o(t)\dot{\hbar}_o(t)}{\hbar_o(t)}\right)\\ &= \alpha_o\left(\dot{P}_g^* - T_g\dot{\Omega}_r - \dot{T}_g\Omega_r - \beta_o\right)\\ &= \alpha_o\dot{P}_g^* - \alpha_o\dot{T}_g\Omega_r - \alpha_o\frac{T_g}{J_o}\left(T_a - K_o\Omega_r - T_g\right) - \alpha_o\beta_o\\ &= \alpha_o\left[\dot{P}_g^* - \frac{1}{J_o}\left(T_gT_a - T_g^2\right) + \frac{K_o}{J_o}T_g\Omega_r - \dot{T}_g\Omega_r - \beta_o\right]\end{aligned} \tag{32}$$

where $\alpha_o = \frac{\partial {M_o}^{-1}}{\partial\left(\frac{\ell_o(t)}{\hbar_o(t)}\right)}\frac{1}{\hbar_o(t)}$ and $\beta_o = \frac{\ell_o(t)\dot{\hbar}_o(t)}{\hbar_o(t)}$. Both α_o and β_o are known signals since $\ell_o(t)$, ${M_o}^{-1}(\cdot)$, $\hbar_o(t)$ and $\dot{\hbar}_o(t)$ are all available. An ideal desired control law is firstly presented to assist the controller design. With the known knowledge of the system dynamics, consider the following ideal controller

$$\dot{T}_g = \frac{1}{\Omega_r}\left[\frac{k_o\gamma_o}{\alpha_o} + \frac{K_o}{J_o}T_g\Omega_r + \dot{P}_g^* - \frac{1}{J_o}\left(T_gT_a - T_g^2\right) - \beta_o\right] \tag{33}$$

where $k_o > 0$ is a positive constant. Then, we can easily obtain that

$$\dot{\gamma}_o = -k_o\gamma_o \tag{34}$$

It means that the ideal controller (33) can ensure the exponential convergence of the transformed tracking error γ_o to zero. Notice that the expression of $\dot{P}_d$ is $\dot{P}_d = \frac{1}{2}n_p\rho\pi R^2C_p^{\max}3V^2\dot{V}$ based on (21) and (20). In order to avoid the knowledge of $\dot{V}$, we use a robust term $\mathrm{sgn}(\alpha_o\gamma_o)B$ to replace $\dot{P}_d$ in (33), and obtain the following desired controller

$$\dot{T}_g = \frac{1}{\Omega_r}\left(\frac{k_o\gamma_o}{\alpha_o} - \beta_o + {\tau_o}^T\xi_o\right) \tag{35}$$

where $\tau_o = [-1/J_o, K_o/J_o, B]^T$, $\xi_o = [T_gT_a - T_g^2, T_g\Omega_r, \text{sgn}(\alpha_o\gamma_o)]^T$, and we have used the upper bound of $\dot{P}_d$. The main results of this ideal controller are summarized in the following lemma.

Lemma 1 *For the transformed error dynamics (32), the transformed tracking error γ_o will converge to zero asymptotically if a desired controller is taken as (35).*

Proof A Lyapunov function candidate is built as

$$V_{\gamma_o} = \frac{1}{2}{\gamma_o}^2 \tag{36}$$

By recalling (32) and (54), its time derivative can be given

$$\begin{aligned}\dot{V}_{\gamma_o} &\le \gamma_o\alpha_o\left[-\dot{T}_g\Omega_r - \frac{T_g}{J_o}\left(T_a - K_o\Omega_r - T_g\right) - \beta_o\right] + |\gamma_o\alpha_o|\,B_o \\ &= \gamma_o\alpha_o\left[-\dot{T}_g\Omega_r + {\tau_o}^T\xi_o - \beta_o\right] \\ &\le -k_o{\gamma_o}^2\end{aligned} \tag{37}$$

which implies that γ_o converges to zero asymptotically [18].

However, the desired controller has two main defects which should be avoided in practice

- The chattering phenomena may appear because the sgn(·) function is discontinuous. In WECS, the chattering phenomena is undesirable because it will reduce the lifetime of wind turbines.
- A priori knowledge of τ_o is needed, which may increase the operation costs.

Aimed at mitigating the chattering phenomena, we use the continuous hyperbolic tangent function $\tanh(\alpha_o\gamma_o/\varepsilon_1)$ to replace the discontinuous $\text{sgn}(\alpha_o\gamma_o)$. Notice that the following inequality holds [19]

$$0 \le |\alpha_o\gamma_o| - \alpha_o\gamma_o\tanh\left(\frac{\alpha_o\gamma_o}{\varepsilon_o}\right) \le \kappa\varepsilon_o \quad \text{for} \quad \alpha_o\gamma_o \in \Re \tag{38}$$

where $\kappa = 0.2758$. Furthermore, since τ_o is unknown, let its estimate be $\hat{\tau}_o$, and the following implementable controller is proposed as

$$\dot{T}_g = \frac{1}{\Omega_r}\left(\frac{k_o\gamma_o}{\alpha_o} - \beta_o + \hat{\tau}_o^T\delta_o\right) \tag{39}$$

where $\delta_o = \left[T_gT_a + T_g^2, T_g\Omega_r, \tanh(\frac{\alpha_o\gamma_o}{\varepsilon_o})\right]^T$. The adaptive law for $\hat{\tau}_o$ is given by

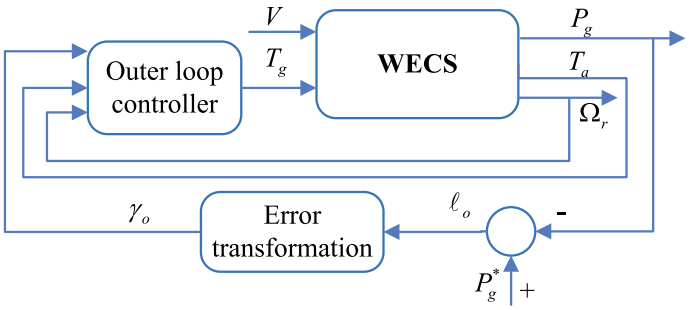

Fig. 4 Controller scheme of the outer loop controller

$$\dot{\hat{\tau}}_o = \Lambda_o \left(\gamma_o \alpha_o \delta_o - \sigma_o \hat{\tau}_o\right) \tag{40}$$

where $\Lambda_o \in \Re^{3\times 3}$, $\sigma_o > 0$.

Figure 4 depicts the control structure of the outer loop controller.

Theorem 1 *For the mechanical subsystem (10) and (12), if we design the outer controller as (39) while the parameter is updated as (40), the imposed performance given in P1 can be achieved.*

Proof Consider the following Lyapunov function candidate

$$V_o = \frac{1}{2}{\gamma_o}^2 + \frac{1}{2}\tilde{\tau}_o^T {\Lambda_o}^{-1} \tilde{\tau}_o \tag{41}$$

where $\tilde{\tau}_o = \hat{\tau}_o - \tau_o$. By recalling (10), (32) and inequality (38), one has

$$\begin{aligned}
\dot{V}_o &= \gamma_o \alpha_o \left(\dot{P}_g^* - T_g \dot{\Omega}_r - \dot{T}_g \Omega_r - \beta_o\right) + \tilde{\tau}_o^T {\Lambda_o}^{-1} \dot{\hat{\tau}}_o \\
&\le \gamma_o \alpha_o \left[-\dot{T}_g \Omega_r - \frac{T_g}{J_o}\left(T_a - K_o \Omega_r - T_g\right) - \beta_o\right] + \left|\gamma_o \alpha_o\right| B_o + \tilde{\tau}_o^T {\Lambda_o}^{-1} \dot{\hat{\tau}}_o \\
&\le \gamma_o \alpha_o \left[-\dot{T}_g \Omega_r + {\tau_o}^T \delta_o - \beta_o\right] + \kappa \varepsilon_o B_o + \tilde{\tau}_o^T {\Lambda_o}^{-1} \dot{\hat{\tau}}_o
\end{aligned} \tag{42}$$

Substituting the outer loop controller (39) and adaptive law (40) into above equation yields

$$\begin{aligned}
\dot{V}_o &\le -k_o {\gamma_o}^2 + ({\tau_o}^T - \hat{\tau}_o^T)\gamma_o \alpha_o \delta_o + \tilde{\tau}_o^T \gamma_o \alpha_o \delta_o + \kappa \varepsilon_o B_o - \sigma_o \tilde{\tau}_o^T \hat{\tau}_o \\
&= -k_o {\gamma_o}^2 + \kappa \varepsilon_o B_o - \sigma_o \tilde{\tau}_o^T \hat{\tau}_o
\end{aligned} \tag{43}$$

Moreover, by completion of squares, one has

$$\dot{V}_o \le -k_o {\gamma_o}^2 - \frac{\sigma_o \|\tilde{\tau}_o\|^2}{2} + \Delta_o \tag{44}$$

where $\Delta_o = \sigma_o \|\tau_o\|^2/2 + \kappa\varepsilon_o B_o$. Hence, $\dot{V}_o < 0$ when $|\gamma_o| > \sqrt{\frac{\Delta_o}{k_o}}$ or $\|\tilde{\tau}_o\| > \sqrt{\frac{2\Delta_o}{\sigma_o}}$ Therefore, based on the standard Lyapunov extension theorem [20, 21], it can be concluded that γ_o and $\tilde{\tau}_o$ are uniformly ultimately bounded (UUB).

Furthermore, since γ_o is bounded, α_o, β_o are also bounded. $\hat{\tau}_o$ is bounded because of $\hat{\tau}_o = \tilde{\tau}_o + \tau_o$ and the boundedness of τ_o. Hence, from (39), we have that the control input T_g is also bounded. Finally, the boundedness of γ_o implies that the imposed performance requirements as given in P1 are achieved.

5 Inner Loop Control

In the inner loop control, the prescribed transient and steady-state performance are also considered. Specifically, the tracking errors are required to satisfy user-defined conditions as

$$\underline{\ell}_{i,T}(t) < \ell_{i,T} < \bar{\ell}_{i,T}(t) \tag{45}$$

$$\underline{\ell}_{i,Q}(t) < \ell_{i,Q} < \bar{\ell}_{i,Q}(t) \tag{46}$$

where $\bar{\ell}_{i,T}(t)$, $\underline{\ell}_{i,T}(t)$ are lower and upper bounds of the tracking error $\ell_{i,T}$ with $\underline{\ell}_{i,T}(t) < 0 < \bar{\ell}_{i,T}(t)$, and $\bar{\ell}_{i,Q}(t)$, $\underline{\ell}_{i,Q}(t)$ are lower and upper bounds of the tracking error $\ell_{i,Q}$ with $\underline{\ell}_{i,Q}(t) < 0 < \bar{\ell}_{i,Q}(t)$.

Aimed at achieving the goal of guaranteed transient performance, we introduce an improved error transformation technique inspired by [22] that can transform the original constrained errors into new unconstrained errors. Specifically, we define

$$\ell_i = \frac{\bar{\ell}_i(t) - \underline{\ell}_i(t)}{\pi} \arctan(\gamma_i) + \frac{\bar{\ell}_i(t) + \underline{\ell}_i(t)}{2} \tag{47}$$

or

$$\gamma_i(t) = \tan\left(\frac{\pi}{2} \times \frac{2\ell_i - \bar{\ell}_i(t) - \underline{\ell}_i(t)}{\bar{\ell}_i(t) - \underline{\ell}_i(t)}\right), \tag{48}$$

where $\tan(\cdot)$, $\arctan(\cdot)$ are the tangent function and inverse tangent function, respectively, $\gamma_i(t)$ is the transformed error. It can be easily verified that the original tracking error ℓ_i strictly increases with respect to the transformed error γ_i, and thus we have $\frac{\partial \ell_i}{\partial \gamma_i} > 0$. Furthermore, from (47), we have

$$\begin{cases} \lim\limits_{\gamma_i \to -\infty} \ell_i = \underline{\ell}_i(t) \\ \lim\limits_{\gamma_i \to \infty} \ell_i = \bar{\ell}_i(t) \end{cases} \tag{49}$$

From (49), it can be concluded that if γ_i exists, the following fact holds

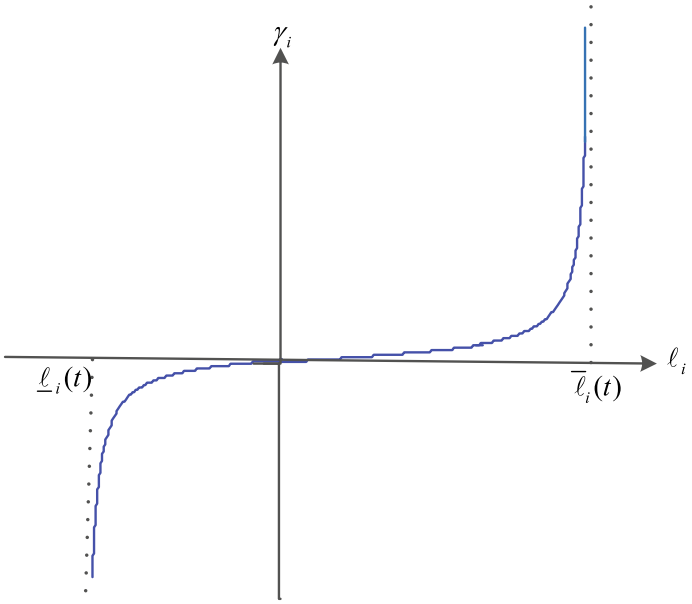

Fig. 5 Graphical illustration of the map from ℓ_i to γ_i

$$\underline{\ell}_i(t) < \ell_i < \bar{\ell}_i(t) \tag{50}$$

which further implies that the guaranteed transient performance in terms of tracking errors is achieved. Therefore, the control objective is converted to finding an inner loop controller that can ensure the boundedness of the transformed error γ_i. The nonlinear mapping between ℓ_i and γ_i is shown in Fig. 5.

Aimed at extracting power from wind as much as possible, the electromagnetic torque should be designed to follow its desired value T^*. The corresponding transformed error of $\ell_{i,T}$ is denoted as $\gamma_{i,T}$. Differentiating $\gamma_{i,T}$ with respect to time and recalling (18), (22) generate

$$\begin{aligned}\dot{\gamma}_{i,T} &= \frac{\partial \gamma_{i,T}}{\partial \ell_{i,T}}\left(-\frac{3}{2}p\frac{U_s L_m}{\Omega_s L_s}\dot{I}_{q,r} - \dot{T}^*\right) + \frac{\partial \gamma_{i,T}}{\partial \bar{\ell}_{i,T}(t)}\dot{\bar{\ell}}_{i,T}(t) + \frac{\partial \gamma_{i,T}}{\partial \underline{\ell}_{i,T}(t)}\dot{\underline{\ell}}_{i,T}(t) \\ &= \alpha_{i,T}\left(-\frac{3}{2}p\frac{U_s L_m}{\Omega_s L_s}\dot{I}_{q,r} - \dot{T}^*\right) + \beta_{i,T}\end{aligned} \tag{51}$$

where $\alpha_{i,T} = \frac{\partial \gamma_{i,T}}{\partial \ell_{i,T}}$ and $\beta_{i,T} = \frac{\partial \gamma_{i,T}}{\partial \bar{\ell}_{i,T}(t)}\dot{\bar{\ell}}_{i,T}(t) + \frac{\partial \gamma_{i,T}}{\partial \underline{\ell}_{i,T}(t)}\dot{\underline{\ell}}_{i,T}(t)$. Because signals $\gamma_{i,T}$, $\ell_{i,T}$, $\bar{\ell}_{i,T}(t)$, $\dot{\bar{\ell}}_{i,T}(t)$, $\underline{\ell}_{i,T}(t)$, $\dot{\underline{\ell}}_{i,T}(t)$ are known, we can easily compute the values of $\alpha_{i,T}$ and $\beta_{i,T}$.

Substituting the dynamics of $I_{q,r}$ given by (16) into (51) and taking the modeling error into account, one has

$$\dot{\gamma}_{i,T} = \alpha_{i,T}\left(f_{i,T}(Z_{i,T}) + g_{i,T}U_{q,r} + d_{i,T}(t)\right) \tag{52}$$

with

$$\begin{aligned} f_{i,T}(Z_{i,T}) &= \frac{3}{2}pL_m\frac{U_sR_r}{\Omega_sL_e}I_{q,r} - \dot{T}^* + \frac{\beta_{i,T}}{\alpha_{i,T}} \\ &\quad + \frac{3}{2}pL_m\frac{U_s}{\Omega_sL_s}\left(\Omega_s - p\Omega_g\right)\left(I_{d,r} + \frac{L_mU_s}{L_e\Omega_s}\right) \\ Z_{i,T} &= [I_{q,r}, I_{d,r}, \Omega_g, \dot{T}^*, \gamma_{i,T}, \alpha_{i,T}]^T \\ g_{i,T} &= -\frac{3}{2}pL_m\frac{U_s}{\Omega_sL_e} \end{aligned} \tag{53}$$

with $d_{i,T}(t) = -\frac{3}{2}p\frac{U_sL_m}{\Omega_sL_s}\varpi_q(t)$ being the system unknown disturbances. Similar to most studies [13], we assume the disturbance term $d_{i,T}$ is bounded.

If the system parameter is available and $d_{i,T}(t) = 0$, a desired control input voltage $U^*_{q,r}$ can be given as

$$U^*_{q,r} = k_{i,T}\frac{\gamma_{i,T}}{\alpha_{i,T}} + {\tau_{i,T}}^T\xi_{i,T} \tag{54}$$

where $\tau_{i,T} = -\left[\frac{1.5pL_mU_sR_r}{\Omega_sL_e}, \frac{1.5pL_mU_s}{L_s}, \frac{1.5pL_m^2U_s^2}{\Omega_sL_eL_s}, -\frac{1.5p^2L_mU_s}{\Omega_sL_s}, \frac{-1.5U_s^2L_m^2p^2}{\Omega_s^2L_sL_e}, -1, 1\right]^T/g_{i,T}$, and $\xi_{i,T} = [I_{q,r}, I_{d,r}, 1, \Omega_gI_{d,r}, \Omega_g, \dot{T}^*, \gamma_{i,T}/\alpha_{i,T}]^T$, $k_{i,T}$ is a positive constant. Thereafter, following lemma shows the system stability with the desired control input $U^*_{q,r}$.

Lemma 2 *Consider the dynamics of $\gamma_{i,T}$ in (52) with $d_{i,T}(t) = 0$. The transformed tracking error $\gamma_{i,T}$ will converge asymptotically to zero if the desired control input $U^*_{q,r}$ is chosen as (54).*

Proof Consider the following Lyapunov candidate

$$V^*_{i,T} = -\frac{1}{2}\frac{\gamma^2_{i,T}}{g_{i,T}} \tag{55}$$

Taking its time derivative and recalling (52) with $d_{i,T} = 0$, we have

$$\dot{V}^*_{i,T} = -\gamma_{i,T}\alpha_{i,T}\left(\frac{f_{i,T}(Z_{i,T})}{g_{i,T}} + U_{q,r}\right) = \gamma_{i,T}\alpha_{i,T}\left({\tau_{i,T}}^T\xi_{i,T} - U_{q,r}\right) \tag{56}$$

Substituting the desired controller (54) into the above equation, we have

$$\dot{V}^*_{i,T} = -k_{i,T}\gamma^2_{i,T} \tag{57}$$

which implies that $\gamma_{i,T}$ converges to zero asymptotically.

The value of $\tau_{i,T}$ is always distinct for different wind turbine systems, and obtaining its value usually needs substantial human and technological efforts. Because of this, it is not economical to extend the proposed controller to various wind turbines. In order to circumvent such issues, the actual value of $\tau_{i,T}$ is supposed to be unknown in the following adaptive controller design. Further, the bounded disturbance term $d_{i,T}$ is assumed to satisfy

$$\left| \frac{d_{i,T}(t)}{g_{i,T}} \right| \leq B_{i,T} \tag{58}$$

with $B_{i,T}$ being a positive unknown constant and $|\cdot|$ being the absolute value operator. Since both $\tau_{i,T}$ and $B_{i,T}$ are unknown, let their estimates to be $\hat{\tau}_{i,T}$ and $\hat{B}_{i,T}$, and we are ready to present the following adaptive control law

$$U_{q,r} = k_{i,T} \frac{\gamma_{i,T}}{\alpha_{i,T}} + \hat{\tau}_{i,T}^T \xi_{i,T} + \tanh\left(\frac{\alpha_{i,T} \gamma_{i,T}}{\varepsilon_{i,T}} \right) \hat{B}_{i,T} \tag{59}$$

with $\tanh(\cdot)$ being the hyperbolic tangent function. The adaptive law for $\hat{\tau}_{i,T}$ is chosen as

$$\dot{\hat{\tau}}_{i,T} = \Lambda_{i,T} \left(\gamma_{i,T} \alpha_{i,T} \xi_{i,T} - \sigma_{i,T1} \hat{\tau}_{i,T} \right) \tag{60}$$

where the learning rate $\Lambda_{i,T} \in \Re^{7\times 7}$ is a positive definite matrix, and $\sigma_{i,T11}$ is a positive constant. Further, the adaptive law for $\hat{B}_{i,T}$ is chosen as

$$\dot{\hat{B}}_{i,T} = l_{i,T} \left(\gamma_{i,T} \alpha_{i,T} \tanh\left(\frac{\alpha_{i,T} \gamma_{i,T}}{\varepsilon_{i,T}} \right) - \sigma_{i,T2} \hat{B}_{i,T} \right) \tag{61}$$

where $l_{i,T}, \sigma_{i,T2} > 0$.

Theorem 2 *Consider the inner loop dynamics characterized by (13) and (14). If the control input voltage $U_{q,r}$ is selected as (59) with adaptive laws (60) and (61), the electromagnetic torque T_{em} can track its desired value T^* with guaranteed performance in terms of tracking error $e_{i,T}$ satisfying (45).*

Proof Consider the following Lyapunov function candidate

$$V_{i,T}^* = -\frac{1}{2} \frac{\gamma_{i,T}^2}{g_{i,T}} + \frac{1}{2} \tilde{\tau}_{i,T}^T \Lambda_{i,T}^{-1} \tilde{\tau}_{i,T} + \frac{1}{2 l_{i,T}} \tilde{B}_{i,T}^2 \tag{62}$$

with $\tilde{\tau}_{i,T} = \hat{\tau}_{i,T} - \tau_{i,T}$, and $\tilde{B}_{i,T} = \hat{B}_{i,T} - B_{i,T}$. Taking the time derivative of $V_{i,T}^*$ generates

$$\dot{V}_{i,T}^* = \gamma_{i,T} \alpha_{i,T} \left(-\frac{f_{i,T}(Z_{i,T})}{g_{i,T}} - U_{q,r} - \frac{d_{i,T}(t)}{g_{i,T}} \right) + \tilde{\tau}_{i,T}^T \Lambda_{i,T}^{-1} \dot{\hat{\tau}}_{i,T} + \frac{1}{l_{i,T}} \tilde{B}_{i,T} \dot{\hat{B}}_{i,T} \tag{63}$$

Using the inequality (38), we have

$$-\gamma_{i,T}\alpha_{i,T}\frac{d_{i,T}(t)}{g_{i,T}} \leq |\gamma_{i,T}\alpha_{i,T}|B_{i,T} \leq \gamma_{i,T}\alpha_{i,T}\tanh\left(\frac{\gamma_{i,T}\alpha_{i,T}}{\varepsilon_{i,T}}\right)B_{i,T} + \kappa\varepsilon_{i,T}B_{i,T} \quad (64)$$

Substituting (64) and (59) into (63) yields

$$\begin{aligned}\dot{V}^*_{i,T} &\leq \gamma_{i,T}\alpha_{i,T}\left({\tau_{i,T}}^T\xi_{i,T} - U_{q,r} + \tanh\left(\frac{\gamma_{i,T}\alpha_{i,T}}{\varepsilon_{i,T}}\right)B_{i,T}\right)\\ &\quad + \tilde{\tau}^T_{i,T}\Lambda^{-1}_{i,T}\dot{\hat{\tau}}_{i,T} + \frac{1}{l_{i,T}}\tilde{B}_{i,T}\dot{\hat{B}}_{i,T} + \kappa\varepsilon_{i,T}B_{i,T}\\ &\leq -k_{i,T}\gamma^2_{i,T} + \tilde{\tau}^T_{i,T}\left(\Lambda^{-1}_{i,T}\dot{\hat{\tau}}_{i,T} - \gamma_{i,T}\alpha_{i,T}\xi_{i,T}\right) + \kappa\varepsilon_{i,T}B_{i,T}\\ &\quad + \tilde{B}_{i,T}\left(\frac{1}{l_{i,T}}\dot{\hat{B}}_{i,T} - \gamma_{i,T}\alpha_{i,T}\tanh\left(\frac{\gamma_{i,T}\alpha_{i,T}}{\varepsilon_{i,T}}\right)\right)\end{aligned} \quad (65)$$

Substituting the adaptive laws (60), (61) and by completion of squares, we have

$$\begin{aligned}\dot{V}^*_{i,T} &\leq -k_{i,T}\gamma^2_{i,T} - \sigma_{i,T1}\tilde{\tau}^T_{i,T}\hat{\tau}_{i,T} - \sigma_{i,T2}\tilde{B}_{i,T}\hat{B}_{i,T} + \kappa\varepsilon_{i,T}B_{i,T}\\ &\leq -k_{i,T}\gamma^2_{i,T} - \frac{\sigma_{i,T1}\|\tilde{\tau}_{i,T}\|^2}{2} - \frac{\sigma_{i,T2}\tilde{B}^2_{i,T}}{2} + \Delta_{i,T}\end{aligned} \quad (66)$$

with $\Delta_{i,T} = \kappa\varepsilon_{i,T}B_{i,T} + \sigma_{i,T1}\|\tau_{i,T}\|^2/2 + \sigma_{i,T2}B^2_{i,T}/2$. Hence, the $\dot{V}^*_{i,T}$ will become negative as long as

$$|\gamma_{i,T}| > \sqrt{\frac{\Delta_{i,T}}{k_{i,T}}} \quad (67)$$

or

$$\|\tilde{\tau}_{i,T}\| > \sqrt{\frac{2\Delta_{i,T}}{\sigma_{i,T1}}} \quad (68)$$

or

$$\left|\tilde{B}_{i,T}\right| > \sqrt{\frac{2\Delta_{i,T}}{\sigma_{i,T2}}} \quad (69)$$

Based on the standard Lyapunov theorem extension [23], $\gamma_{i,T}$, $\tilde{\tau}_{i,T}$ and $\tilde{B}_{i,T}$ are bounded.

According to the properties of error transformation, the boundedness of $\gamma_{i,T}$ concludes that the guaranteed performance described by (45) is achieved, and thus $e_{i,T}$ is bounded. The reference T^* generated by the MPPT algorithm is bounded. It thus

follows that T_{em} is bounded. Since $\hat{\tau}_{i,T} = \tilde{\tau}_{i,T} + \tau_{i,T}$, and $\tau_{i,T}$ is bounded from definition, we have that $\hat{\tau}_{i,T}$ is bounded as well. Since $\hat{B}_{i,T} = \tilde{B}_{i,T} + B_{i,T}$, and $B_{i,T}$ is bounded from definition, we have that $\hat{B}_{i,T}$ is also bounded.

The value of desired reactive power Q^* is determined by grid needs, e.g., a specified amount of reactive power compensated in grid can improve the role of the grid power factor, lower power transformer and transmission line losses. In this chapter, for analysis convenience, the desired reactive power Q^* is assumed to be a known signal, and the control objective is to track a desired Q^* with guaranteed performance, i.e., to obtain the tracking error $e_{i,Q}$ satisfying (46). By recalling (19), the time derivative of $\gamma_{i,Q}$ can be obtained as

$$\begin{aligned}\dot{\gamma}_{i,Q} &= \frac{\partial \gamma_{i,Q}}{\partial \ell_{i,Q}}\left(-\frac{3U_s L_m}{2L_s}\dot{I}_{d,r} - \dot{Q}^*\right) + \frac{\partial \gamma_{i,Q}}{\partial \bar{\ell}_{i,Q}(t)}\dot{\bar{\ell}}_{i,Q}(t) + \frac{\partial \gamma_{i,Q}}{\partial \underline{\ell}_{i,Q}(t)}\dot{\underline{\ell}}_{i,Q}(t) \\ &= \alpha_{i,Q}\left(-\frac{3U_s L_m}{2L_s}\dot{I}_{d,r} - \dot{Q}^*\right) + \beta_{i,Q} \end{aligned} \tag{70}$$

where $\alpha_{i,Q} = \frac{\partial \gamma_{i,Q}}{\partial \ell_{i,Q}}$ and $\beta_{i,Q} = \frac{\partial \gamma_{i,Q}}{\partial \bar{\ell}_{i,Q}(t)}\dot{\bar{\ell}}_{i,Q}(t) + \frac{\partial \gamma_{i,Q}}{\partial \underline{\ell}_{i,Q}(t)}\dot{\underline{\ell}}_{i,Q}(t)$, which are available as feedback signals.

By recalling (15), (70) and considering the modeling error, we have

$$\dot{\gamma}_{i,Q} = \alpha_{i,Q}\left(f_{i,Q}(Z_{i,Q}) + g_{i,Q}U_{d,r} + d_{i,Q}(t)\right) \tag{71}$$

with

$$\begin{aligned} f_{i,Q}(Z_{i,Q}) &= \frac{3U_s L_m R_r}{2L_e} I_{d,r} - \frac{3U_s L_m}{2L_s}\left(\Omega_s - p\Omega_g\right) I_{q,r} - \dot{Q}^* + \frac{\gamma_{i,Q}}{\alpha_{i,Q}} \\ Z_{i,Q} &= [I_{q,r}, I_{d,r}, \Omega_g, \dot{Q}^*, \gamma_{i,Q}, \alpha_{i,Q}]^T \\ g_{i,Q} &= -\frac{3U_s L_m}{2L_e} \end{aligned} \tag{72}$$

with $d_{i,Q}(t) = -\frac{3U_s L_m \varpi_d(t)}{2L_s}$ being the bounded disturbance term embodying modeling errors in the dynamics of $\ell_{i,Q}$. To facilitate the reactive power control design, it can be observed that

$$-\frac{f_{i,Q}(Z_{i,Q})}{g_{i,Q}} = {\tau_{i,Q}}^T \xi_{i,Q} \tag{73}$$

where $\tau_{i,Q} = -[1.5U_s L_m R_r/L_e, -1.5U_s L_m \Omega_s/L_s, 1.5U_s L_m \ \ p/L_s, -1, 1]^T/g_{i,Q}$, and $\xi_{i,Q} = [I_{d,r}, I_{q,r}, \Omega_g I_{q,r}, \dot{Q}^*, \gamma_{i,Q}/\alpha_{i,Q}]^T$. Moreover, assume that the disturbance term $d_{i,Q}(t)$ is bounded such that

$$\left|\frac{d_{i,Q}(t)}{g_{i,Q}}\right| \leq B_{i,Q} \tag{74}$$

Since both $\tau_{i,\varrho}$ and $B_{i,\varrho}$ are unknown, let their estimates to be $\hat{\tau}_{i,\varrho}$ and $\hat{B}_{i,\varrho}$, we propose the following input $U_{d,r}$

$$U_{d,r} = k_{i,\varrho}\frac{\gamma_{i,\varrho}}{\alpha_{i,\varrho}} + \hat{\tau}_{i,\varrho}^{T}\xi_{i,\varrho} + \tanh\left(\frac{\alpha_{i,\varrho}\gamma_{i,\varrho}}{\varepsilon_{i,\varrho}}\right)\hat{B}_{i,\varrho} \tag{75}$$

with $k_{i,\varrho}$ being a user-defined positive constant. The adaptive laws for $\hat{\tau}_{i,\varrho}$ and $\hat{B}_{i,\varrho}$ are given by

$$\begin{aligned}\dot{\hat{\tau}}_{i,\varrho} &= \Lambda_{i,\varrho}\left(\gamma_{i,\varrho}\alpha_{i,\varrho}\xi_{i,\varrho} - \sigma_{i,\varrho 1}\hat{\alpha_o}\right)\\ \dot{\hat{B}}_{i,\varrho} &= l_{i,\varrho}\left(\gamma_{i,\varrho}\alpha_{i,\varrho}\tanh\left(\frac{\alpha_{i,\varrho}\gamma_{i,\varrho}}{\varepsilon_{i,\varrho}}\right) - \sigma_{i,\varrho 2}\hat{B}_{i,\varrho}\right)\end{aligned} \tag{76}$$

where the learning rate $\Lambda_{i,\varrho} \in \Re^{5\times 5}$ is a positive definite matrix, and $l_{i,\varrho}$ is a positive constant.

The stability and control performance of the reactive power closed-loop system is given in the following theorem.

Theorem 3 *Consider the inner loop control characterized by (13) and (14). If the control voltage $U_{d,r}$ is designed by (75) with adaptive laws (76), the reactive power Q can track its desired value Q^* with guaranteed performance in terms of tracking error $\ell_{i,\varrho}$ satisfying (46).*

Proof The proof is similar to Theorem 2 and thus omitted here.

6 Validation Results

To validate the proposed inner loop control and outer loop control, we have conducted numerical analysis using NREL FAST code [24] on the NREL WP 1.5 MW wind turbine, which has three blades on a horizontal axis [25, 26]. The parameters of the wind turbine are given in Table 1.

We use the FAST module in the Simulink environment as shown in Fig. 6. We choose the following system parameters in our validation: air density $\rho =$

Table 1 Parameters of wind turbine

Number of blades	3
Rotor radius	35 m
Hub height	84.3 m
Rated power	1.5 MW
Turbine total inertia	4.4532×10^5 kg m^2

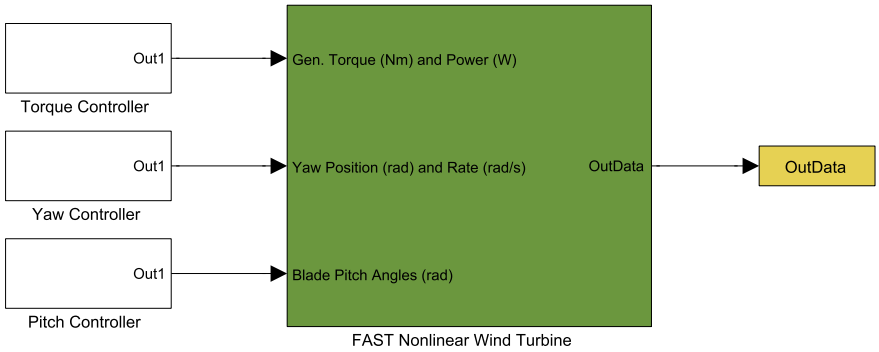

Fig. 6 FAST simulator block

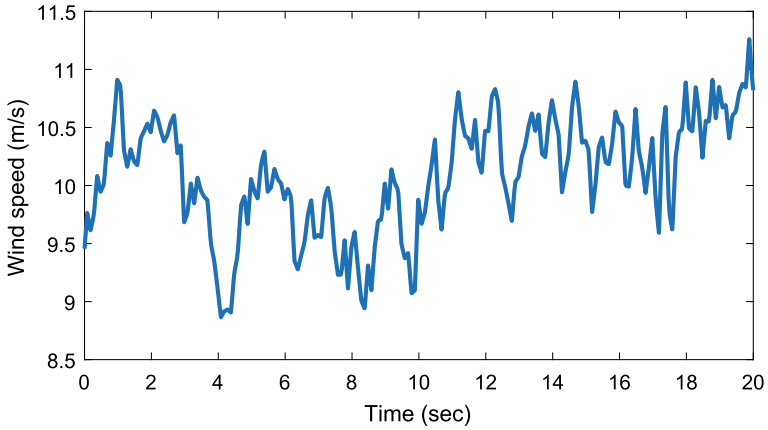

Fig. 7 Wind profile for outer loop control

$1.225\,\mathrm{kg/m^3}$, ratio $n_p = 0.9$, maximum power ratio $C_p^{\max} = 0.412$. The controller parameters are listed as follows: $k_o = 5$, $\Lambda_o = \mathrm{diag}(10^{-25}, 10^{-15}, 10^{-3})$, $\sigma_o = 10$, $\varepsilon_o = 10$.

The wind speed used in this test is given in Fig. 7. It is generated by the TurbSim [27] with the mean wind speed as 9.5 m/s and turbulence intensity as 15%.

The tracking error performance is depicted in Fig. 8, which can be observed that our proposed outer loop controller can ensure the imposed performance requirements. Figure 9 shows the output power trajectory of the generator. It can be observed that the power output can follow the maximum available power from wind. Finally, Fig. 10 depicts the generator torque input.

For the inner loop control, in order to consider the external noises, two Gaussian distribution noises with standard deviations 0.1 and 0.5 are added in the dynamics of $I_{d,r}$ and $I_{q,r}$. In this case study, the generated wind speed is shown in Fig. 11, which is also created using the Kaimal turbulence model with a mean value of 6 m/s

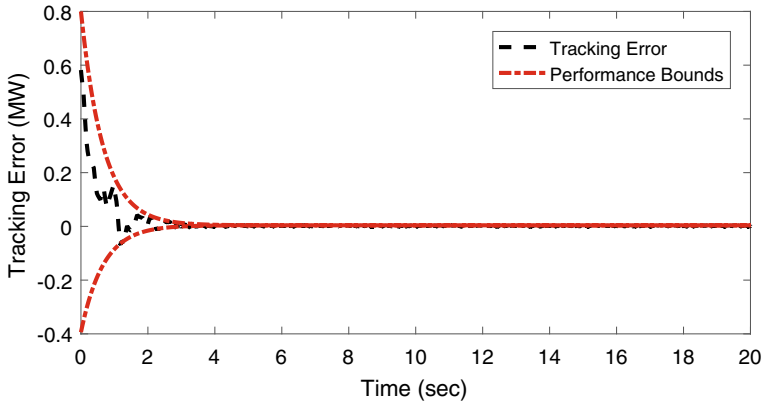

Fig. 8 Tracking error ℓ_o

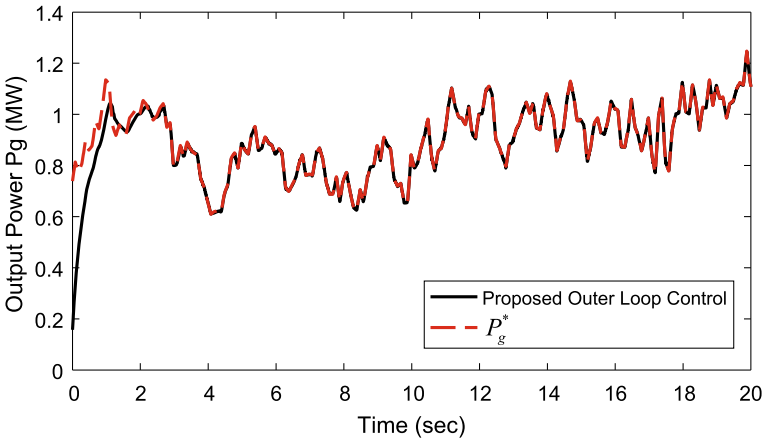

Fig. 9 Generator output power

and turbulence intensity of 10%. To be more realistic, the temporal evolution of the electrical parameters (resistances, inductances), varying from their nominal values is considered as shown in Fig. 12.

One of the control goal is to drive electromagnetic torque T_{em} to track T^* by setting $k_{opt} = 0.2357$, with tracking error $\ell_{i,T}$ satisfying predefined constraints. The corresponding upper bound $\bar{\ell}_T(t)$ is determined as $9 \times \exp(-2t) + 1$ along with the lower bound as $-149 \times \exp(-3t) - 1$. Moreover, control parameters in control of electromagnetic torque are listed as follows: $k_{i,T} = 3 \times 10^{-4}$, $\Lambda_{i,T} = \text{diag}\{10^{-6}, 2 \times 10^{-6}, 1, 2 \times 10^{-10}, 10^{-5}, 3 \times 10^{-7}, 3 \times 10^{-7}\}$, $\sigma_{i,T11} = 2 \times 10^{-5}$, $l_{i,T} = 0.01$, $\sigma_{i,T2} = 3$, $\varepsilon_{i,T} = 2$.

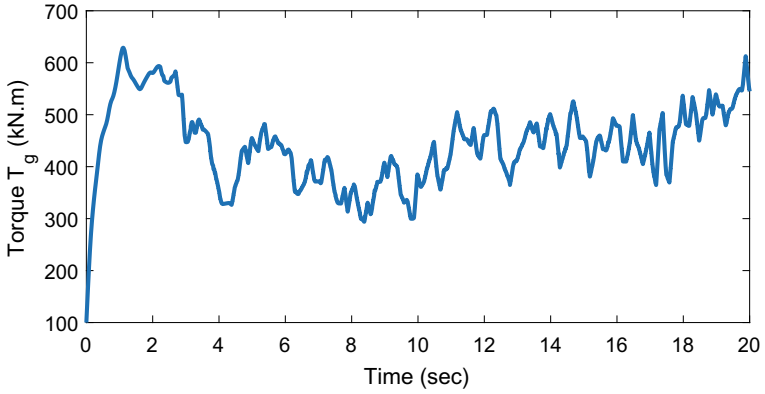

Fig. 10 Generator torque

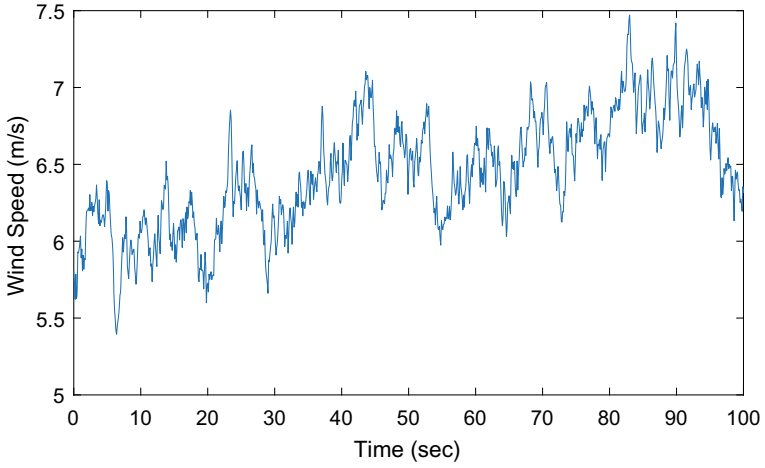

Fig. 11 Wind speed profile

Figure 13 depicts the electromagnetic torque and its desired value T^*, which shows good tracking performance. The tracking error $\ell_{i,T}$ with its performance bounds is given in Fig. 14. It can be observed that the prescribed performance is achieved.

The desired reactive power is given by $Q^* = 1000 + 30\sin(0.1t)$. One of the control goals is to drive the the reactive power to follow this desired power with tracking error $\ell_{i,Q}$ satisfying predefined constraints. The corresponding upper bound $\bar{\ell}_Q(t)$ is determined as $3.5 \times \exp(-2t) + 1$ along with the lower bound as $-118.5 \times \exp(-5t) - 1$. Moreover, control parameters in control of reactive power are listed as follows: $k_{i,Q} = 4 \times 10^{-7}$, $\Lambda_{i,Q} = \text{diag}\{10^{-7}, 9 \times 10^{-8}, 4 \times 10^{-12}, 0.001, 10^{-5}\}$, $\sigma_{Q1} = 2$, $l_{i,Q} = 5 \times 10^{-7}$, $\sigma_{Q2} = 1$, $\varepsilon_Q = 5$.

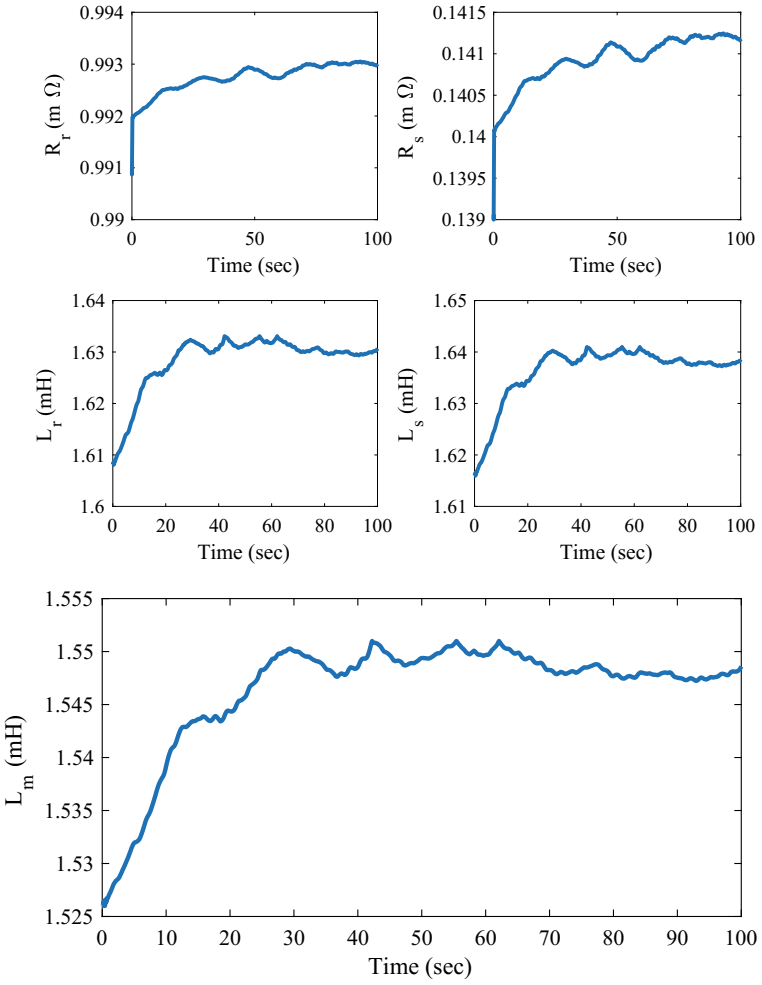

Fig. 12 Temporal evolution of the electromagnetic parameters

Figure 15 shows the reactive power and its desired value Q^*, and the corresponding tracking error $\ell_{i,\varrho}$ along with its performance bounds is plotted in Fig. 16. It can be observed that the corresponding prescribed performance can also be ensured.

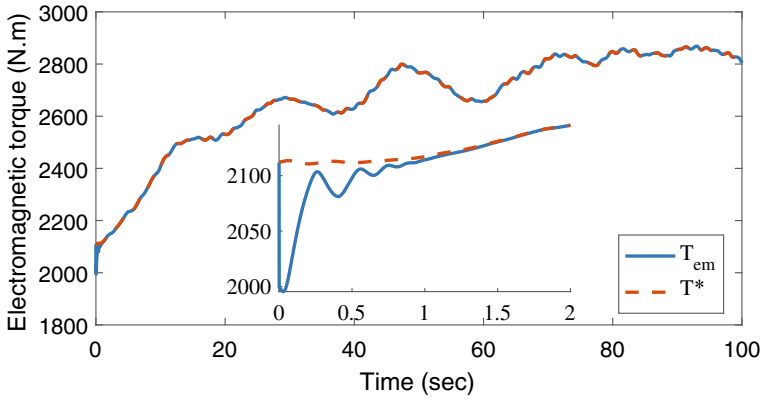

Fig. 13 Electromagnetic torque and its reference

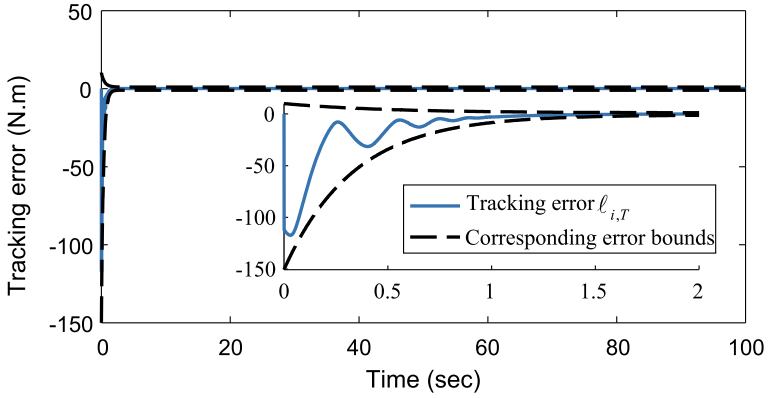

Fig. 14 Tracking error $\ell_{i,T}$ along with its bounds

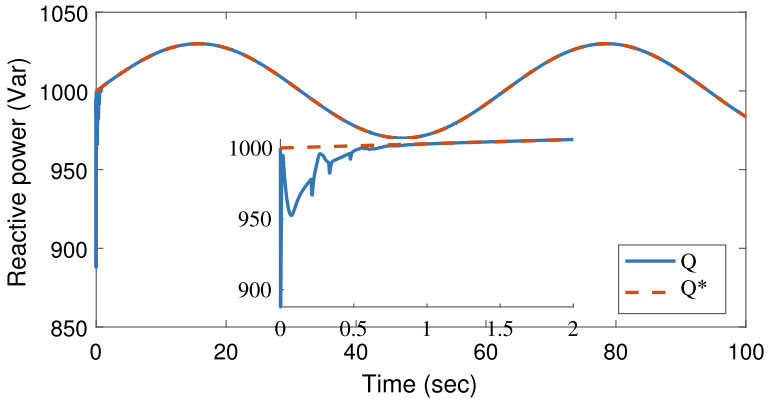

Fig. 15 Reactive power and its reference

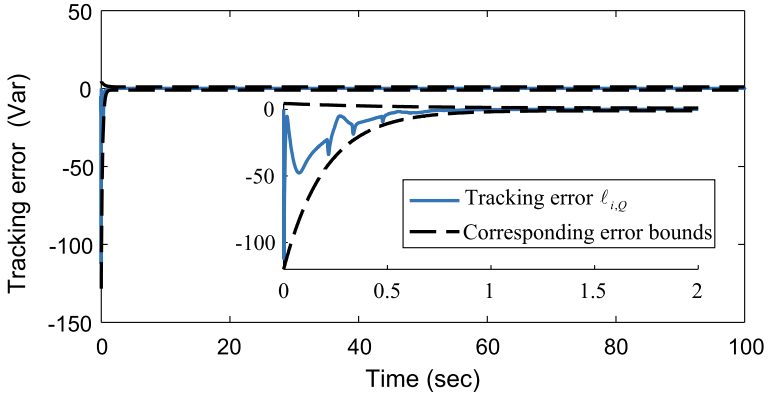

Fig. 16 Tracking error $\ell_{i,Q}$ along with its bounds

7 Conclusion

We have proposed an adaptive guaranteed performance controller for WECS equipped with DFIG. The WECS comprises the outer loop control concerning the aeroturbine mechanical subsystem, and the inner loop control concerning the electrical subsystem. Because the aeroturbine runs much slower than electrical subsystem, the stability analysis in the outer control loop and inner control loop is addressed separately. With the help of error transformation, our proposed method is capable of quantifying and further guaranteeing the system performance on both transient and steady state stages.

References

1. Bose B (2010) Global warming: energy, environmental pollution, and the impact of power electronics. IEEE Ind Electron Mag 4(1):6–17
2. Kaldellis JK (2008) The wind potential impact on the maximum wind energy penetration in autonomous electrical grids. Renew Energy 33(7):1665–1677
3. Joselin Herbert GM, Iniyan S, Sreevalsan E, Rajapandian S (2007) A review of wind energy technologies. Renew Sustain Energy Rev 11(6):1117–1145
4. Todeschini G, Emanuel AE (2011) Transient response of a wind energy conversion system used as active filter. IEEE Trans Energy Convers 26(2):522–531
5. Munteanu I, Cutululis NA, Bratcu AI, Ceanga E (2005) Optimization of variable speed wind power systems based on a LQG approach. Control Eng Pract 13(7):903–912
6. Bououden S, Chadli M, Filali S, Hajjaji AE (2012) Fuzzy model based multivariable predictive control of a variable speed wind turbine: LMI approach. Renew Energy 37(1):434–439
7. Boukhezzar B, Siguerdidjane H (2009) Nonlinear control with wind estimation of a DFIG variable speed wind turbine for power capture optimization. Energy Convers Manag 50(4):885–892

8. Benbouzid M, Beltran B, Amirat Y, Yao G, Han J, Mangel H (2014) Second-order sliding mode control for DFIG-based wind turbines fault ride-through capability enhancement. ISA Trans 53(3):827–833
9. Meng W, Yang Q, Ying Y, Sun Y, Yang Z, Sun Y (2013) Adaptive power capture control of variable-speed wind energy conversion systems with guaranteed transient and steady-state performance. IEEE Trans Energy Convers 28(3):716–725
10. Meng W, Yang Q, Sun Y (2016) Guaranteed performance control of DFIG variable-speed wind turbines. IEEE Trans Control Syst Technol 24(6):2215–2223
11. Beltran B, Ahmed-Ali T, Benbouzid M (2009) High-order sliding-mode control of variable-speed wind turbines. IEEE Trans Ind Electron 56(9):3314–3321
12. Evangelista C, Valenciaga F, Puleston P (2013) Active and reactive power control for wind turbine based on a MIMO 2-sliding mode algorithm with variable gains. IEEE Trans Energy Convers 28(3):682–689
13. Valenciaga F, Puleston PF, Spurgeon SK (2009) A geometric approach for the design of MIMO sliding controllers. Application to a wind-driven doubly fed induction generator. Int J Robust Nonlinear Control 19(1):22–39
14. Boukhezzar B, Lupu L, Siguerdidjane H, Hand M (2007) Multivariable control strategy for variable speed, variable pitch wind turbines. Renew Energy 32(8):1273–1287
15. Kumar A, Stol K (2010) Simulating feedback linearization control of wind turbines using high-order models. Wind Energy 13(5):419–432
16. Beltran B, El Hachemi Benbouzid M, Ahmed-Ali T (2012) Second-order sliding mode control of a doubly fed induction generator driven wind turbine. IEEE Trans Energy Convers 27(2):261–269
17. Bechlioulis CP, Rovithakis GA (2008) Robust adaptive control of feedback linearizable mimo nonlinear systems with prescribed performance. IEEE Trans Autom Control 53(9):2090–2099
18. Slotine JJE, Li W et al (1991) Applied nonlinear control. Prentice-Hall Englewood Cliffs, NJ
19. Chen M, Ge SS, Ren B (2011) Adaptive tracking control of uncertain mimo nonlinear systems with input constraints. Automatica 47(3):452–465
20. Narendra K, Annaswamy A (1987) A new adaptive law for robust adaptation without persistent excitation. IEEE Trans Autom Control 32(2):134–145
21. Yang Q, Jagannathan S (2012) Reinforcement learning controller design for affine nonlinear discrete-time systems using online approximators. IEEE Trans Syst Man Cybern Part B Cybern 42(2):377–390
22. Bechlioulis CP, Rovithakis GA (2014) A low-complexity global approximation-free control scheme with prescribed performance for unknown pure feedback systems. Automatica 50(4):1217–1226
23. Lewis FL, Jagannathan S, Yesildirak A (1999) Neural network control of robot manipulators and non-linear systems. Taylor & Francis, Philadelphia, PA
24. National Renewable Energy Laboratory, Golden, CO. (2007, Feb). http://wind.nrel.gov/designcodes/simulators/fast/
25. Beltran B, Ahmed-Ali T, El Hachemi Benbouzid M (2008) Sliding mode power control of variable-speed wind energy conversion systems. IEEE Trans Energy Convers 23(2):551–558
26. Buhl Jr ML, Manjock A (2006) A comparison of wind turbine aeroelastic codes used for certification. Natl Renew Energy Lab, Golden, CO, NREL/CP-500-39113
27. Jonkman BJ, Buhl Jr ML, Turbsim user's guide. Technical Report NREL/TP-500-41136. National Renewable Energy Laboratory (NREL), Golden, CO. http://wind.nrel.gov/designcodes/simulators/fast/